Supporting Information for

Synthesis of high melting point TiN mesocrystal powders by a metastable state strategy

Maoqiao Xiang, [a] Miao Song, [ab] Qingshan Zhu,*[ab] Yafeng Yang, *[a] Shaofu Li,[a] Chaoquan Hu,[a] Pengpeng Lv,[a] Feng Pan [a] and Yu Ge [a]

[a] State Key Laboratory of Multiphase Complex Systems, Institute of Process Engineering, Chinese Academy of Sciences, P.O. Box 353, Beijing 100190, PR China

[b] University of Chinese Academy of sciences, Beijing 100049, PR China

***Corresponding author**: Qingshan Zhu; E-mail: qszhu@ipe.ac.cn; Tel:+86-010-62536108; Fax: +86-010-62536108;

***Corresponding author**: Yafeng Yang; E-mail: yfyang@ipe.ac.cn; Tel: +86-010-82544907; Fax: +86-010-82544907.

I. Preparing the metastable $TiCl_2$ powders

The Ti powder (38 um, purity 99.8%) and $TiCl_4$ (purity 99.9%) were bought from Xing Rong Yuan Technology Co., Ltd. Beijing, China and Macklin Inc. Shanghai, China. A fluidized bed process was employed to prepare the metastable $TiCl_2$ powder (Fig.S1.a). This is because the fluidized bed process has the advantage of high heat efficiency and mass transfer property and is suitable for mass production. Firstly, the Ti powders (6.0 g) were put in the fluidized bed. Secondly, Ar was used to wash the fluidized bed (Ar = 300 ml/min, 40 min) for eliminating air at about 150 ^oC. Then, the temperatures of the $TiCl_4$ container and the fluidized bed (Fig.S1) were increased to 70 ^oC and 600 ^oC, respectively. Meanwhile, the flow velocity of Ar was 600 ml/min. After 3 hours the black $TiCl_2$ powders were obtained.

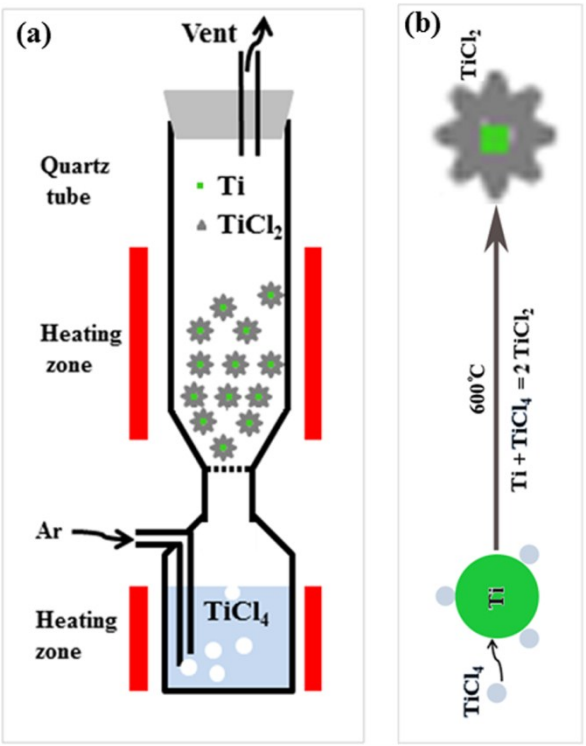

Fig.S1. (a) Schematic diagram of preparing $TiCl_2$ precursor by fluidized bed process. (b) Schematic diagram of synthetic process of $TiCl_2$.

However, the synthesized $TiCl_2$ precursors were $TiCl_2$ and Ti mixtures (Fig.S2.a). The Ti powders were uniformly covered by the $TiCl_2$ film (Fig.S2.b and c). This is because the $TiCl_2$(s) formed on the surface of Ti(s) powder at early stage acted as the

barrier for further reaction between $TiCl_4$(g) and Ti(s) (Fig.S2.a.2). However, our design idea is based on the gaseous $TiCl_2$(g) to synthesize TiN powders. The vapor pressure of Ti(s) is much lower than that of $TiCl_2$(s). Hence, the residual Ti cores in the $TiCl_2$ powders have little influence on the TiN synthesis.

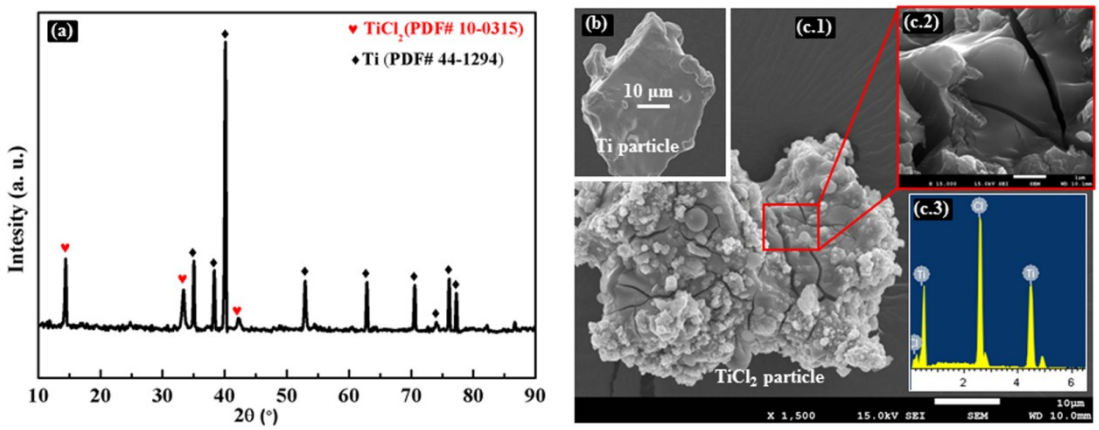

Fig.S2. (a) XRD pattern of the synthesized black $TiCl_2$ powders; (b) SEM image of the Ti particle before reaction; (c.1) and (c.1) SEM of images of the synthesized black $TiCl_2$ particle; (c.3) EDS pattern of the $TiCl_2$ powder.

II. Synthesizing the TiN mesocrystal powders

The synthesized $TiCl_2$ powders were transferred in to a special quartz crucible located in a tube furnace (Fig. S3). The solid state $TiCl_2$(s) powders were sublimated into gas state $TiCl_2$(g) and transported to the reaction zones. Meanwhile, the metastable gaseous $TiCl_2$(g) could release fresh Ti atoms by its disproportionate reaction or react with nitrogen sources directly to form TiN powders. The synthesis temperatures were varied from 750 °C to 900 °C. The synthesis time was 30 minutes. Different nitrogen sources (ammonia gas (NH_3) and nitrogen (N_2)) were investigated.

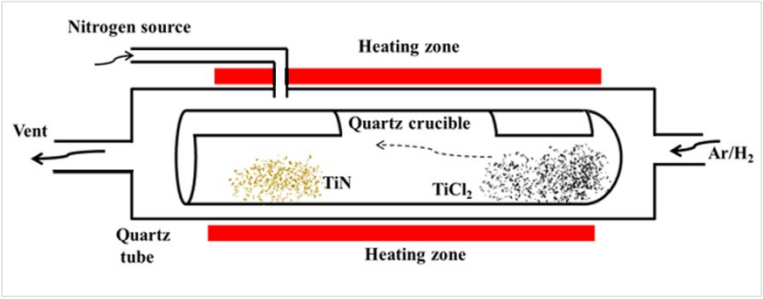

Fig.S3. Schematic diagram of preparing TiN mesocrystal powders.

III. The phase analysis and elemental analysis

The elemental analysis were detected by the field emission scanning electron microscopy (FESEM, Semicon, JSM-7001F) equipped with an energy dispersive spectroscopy (EDS) detector, and the results are shown in Fig.S4. The samples were coated by a thin Pt layer (20 mA, 30 seconds) in order to obtain a better conductive surface. The N element, Ti element, and Cl element were detected in all samples, and the content of Cl element decreased as the temperature increased. The phase compositions of all samples in the $TiCl_2$-NH_3 system and $TiCl_2$-N_2 system were identified using an X'Pert PRO X-ray diffractometer (XRD, PANalytical, the Netherlands) with the Cu Kα (1.542 Å) radiation in the range 2θ from 10° to 90° with a scanning speed of 1° min^{-1}, and the results are shown in Fig.S5. The peaks fitting, phase identification and refinement of XRD profile were examined by PANalytical X'Pert HighScore Plus software. The diffraction peaks are indexed well to a face-centered cubic (FCC) structure with space group of Fm-3m (JCPDS Card No. 38-1420). No other diffraction peaks are detected, indicating the high purity of TiN. The intensities of peaks increased with increasing temperature. The average crystallite size of TiN powders were calculated using Debye–Scherrer formula,[1] i.e. $D = \frac{0.9\lambda}{\beta cos\theta}$, where, D and λ are the crystallite size and the wavelength of Cu-Kα radiation, respectively. θ is the Bragg diffraction angle, and β is the full-width-at-half-maximum (FWHM) of the peaks in radians. The crystallite sizes of the TiN powders are shown in table S1. The crystallite sizes o increased from 28.45 nm to 63.41 nm as the temperature increased from 750 °C to 900 °C in the $TiCl_2$-NH_3 system.

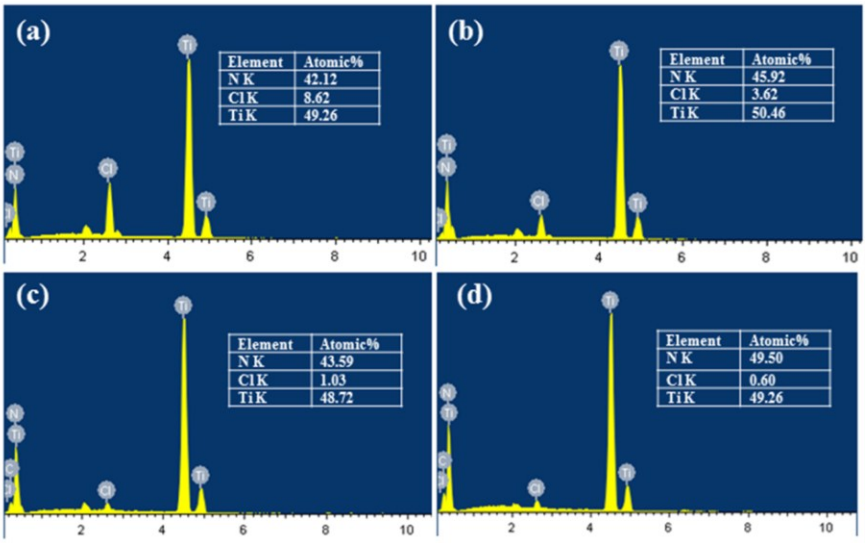

Fig.S4 The EDS results of the synthesized TiN powders in the $TiCl_2$-NH_3 system at different temperatures: (a) 750 °C, (b) 800 °C, (c) 850 °C, (d) 900 °C.

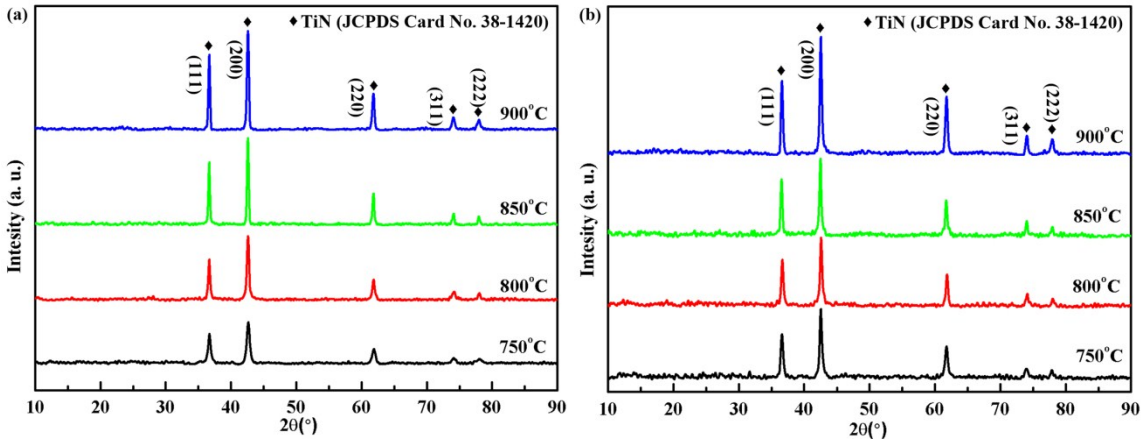

Fig.S5 (a) The XRD patterns of the synthesized TiN powders in the $TiCl_2$-NH_3 system from 750 °C to 900 °C; (b) the XRD patterns of the synthesized TiN powders in the $TiCl_2$-N_2 system from 750 °C to 900 °C.

Table S. 1. Crystallite size of the obtained samples in the $TiCl_2$-NH_3 and $TiCl_2$-N_2 system from 750 °C to 900 °C.

Temperature (°C)		750 °C	800 °C	850 °C	900 °C
D (nm)	$TiCl_2$-NH_3	28.45	38.65	54.82	63.41
	$TiCl_2$-N_2	22.13	33.74	47.25	56.29

IV. Microstructure and specific surface area characterization of obtained TiN powders

Microstructures of all samples were characterized by the field emission scanning electron microscopy (FESEM, Semicon, JSM-7001F). The sizes of the obtained TiN powders were measured by Nano Measurer 1.2 software. All transmission electron microscopy (TEM, 80-200kV/JEM-2100PLUS, Japan) samples were prepared by placing a drop of a solution contained TiN powders onto a carbon coated copper grid. The TEM images were analyzed by the Digital Micrograph software (Ganta, USA). The orientations and morphologies of 2 to 15 nm particles were identified by the fast Fourier transform (FFT) patterns of high resolution transmission electron microscopy (HRTEM) lattice images. Specific surface areas of the obtained samples were determined by nitrogen physical sorption BET measurements using AUTOSORB-IQ-XR-C (Quantachrome, USA) device. The results are shown in Table S2.

Table S.2. Specific surface areas of the obtained samples.

Temperature	$TiCl_2$-NH_3-xAr systems	
	$x = 0$	$x = 2$
750 °C	31.24	36.25
800 °C	23.15	25.96
850 °C	17.34	21.45
900 °C	16.59	18.75

V. The thermodynamic calculation and analysis

The thermodynamic calculation in this experiment was conducted by HSC Chemistry 6.0 software (Outokumpu Research Oy, Finland). In theory, the metastable $TiCl_2$ can be converted into Ti, $TiCl_3$ and $TiCl_4$ by itself disproportionation in a certain range of temperature. Meanwhile, the $TiCl_3$ and $TiCl_4$ can also be reduced to $TiCl_2$ by Ti powders or H_2. And each of them can be nitrided by NH_3 or N_2 with H_2 to

form TiN. In addition, the NH_3 can be decomposed into N_2 and H_2. Hence, there are 17 possible reaction equations (Eqs.) in the system (Table S.3).

Table S.3. The possible reactions in the $TiCl_2$-NH_3 system.

Chemical reaction equation	Numbers
$TiCl_{2(g)} + H_{2(g)} = Ti_{(s)} + 2HCl_{(g)}$	1
$TiCl_{3(g)} + 3/2H_{2(g)} = Ti_{(s)} + 3HCl_{(g)}$	2
$TiCl_{3(g)} + 1/2H_{2(g)} = TiCl_{2(g)} + HCl_{(g)}$	3
$TiCl_{4(g)} + 2H_{2(g)} = Ti_{(s)} + 4HCl_{(g)}$	4
$TiCl_{4(g)} + H_{2(g)} = TiCl_{2(g)} + 2HCl_{(g)}$	5
$TiCl_{4(g)} + 1/2H_{2(g)} = TiCl_{3(g)} + 2HCl_{(g)}$	6
$TiCl_{2(g)} = 1/3Ti_{(s)} + 2/3TiCl_{3(g)}$	7
$TiCl_{2(g)} = 1/2Ti_{(s)} + 1/2TiCl_{4(g)}$	8
$TiCl_{3(g)} = 1/2TiCl_{2(g)} + 1/2TiCl_{4(g)}$	9
$TiCl_{3(g)} = 1/4Ti_{(s)} + 3/4TiCl_{4(g)}$	10
$NH_{3(g)} = 3/2H_{2(g)} + 1/2N_{2(g)}$	11
$TiCl_{2(g)} + NH_{3(g)} = TiN_{(s)} + 2HCl_{(g)} + 1/2H_{2(g)}$	12
$TiCl_{3(g)} + NH_{3(g)} = TiN_{(s)} + 3HCl_{(g)}$	13
$TiCl_{4(g)} + 4/3NH_{3(g)} = TiN_{(s)} + 4HCl_{(g)} + 1/6N_{2(g)}$	14
$Ti_{(s)} + 1/2N_{2(g)} = TiN_{(s)}$	15
$Ti_{(s)} + NH_{3(g)} = TiN_{(s)} + 3/2H_{2(g)}$	16
$TiCl_{2(g)} + 1/2N_{2(g)} + H_{2(g)} = TiN_{(s)} + 2HCl_{(g)}$	17

Fig. S6 shows Gibbs free energy (ΔG) variations and equilibrium constant (K) variations of the 17 possible reactions. From the point of view of thermodynamics, the reaction with small ΔG and big K is the feasible reaction. The Eq.11 shows negative ΔG and positive K, implying that the NH_3 can be decomposed into N_2 and H_2. In order to verify this reaction, the reaction tail gas of $TiCl_2$-NH_3 system from 750 ^oC to 900 ^oC was monitored by hydrogen detector. And we found that the hydrogen indeed existed in all process. Hence, the hydrogen also plays a role in the $TiCl_2$-NH_3 system

for synthesizing TiN powders. The Eqs. (1) to (6) have big postive ΔG and very small K, indicating that the $TiCl_2(g)$, $TiCl_3(g)$ and $TiCl_4(g)$ can hardly be reduced by H_2. The Eqs. (7) and (8) show more negative ΔG values and bigger K values than the Eqs. (9) and (10), indicating that the conversion of $TiCl_2(g)$ into fresh Ti(s) is relatively feasible pathway ($TiCl_2(g)\rightarrow Ti(s)+ TiCl_3(g)$, $TiCl_2(g)\rightarrow Ti(s)+ TiCl_4(g)$) than the conversion of $TiCl_3(g)$. Hence, the $TiCl_4(g)$ and $TiCl_3(g)$ by-products are formed inevitably in this system. For the reaction (11) to (17), they show negative ΔG and positive K, implying that the fresh Ti(s), $TiCl_2(g)$, $TiCl_3(g)$, and $TiCl_4(g)$ can be nitrided by NH_3 or N_2 to form TiN. The nitridation reactions of Ti(s) (Eqs.15 and 16) show the very negative ΔG and the biggest K, indicating that the Ti(s) →TiN(s) reactions are the most feasible reactions. Meanwhile, the Eqs.12 and 17 show the second low negative ΔG and the second big K, indicating that the $TiCl_2(s)$ →TiN(s) reactions are the second feasible reactions. In addition, it is well known that the pure TiN can only be synthesized at least 1000 ^oC in the $TiCl_4(g)$-N_2-H_2 system. Hence, based on the calculation results, the reaction orders can be describes as: Ti(s)→TiN > $TiCl_2$→TiN > $TiCl_3$→TiN > $TiCl_4$→TiN. It is worth to mention that the reactions between the fresh Ti(s) and $TiCl_4(g)$, $TiCl_3(g)$ have not been taken into account because the fresh Ti(s) from the disproportionation can be consumed immediately by NH_3 or N_2. Therefore, the possible synthesis pathways in the $TiCl_2(g)$-NH_3 system can be divided in to two parts: $TiCl_2(g)\rightarrow Ti(s)\rightarrow TiN(s)$, $TiCl_2(g)\rightarrow TiN(s)$.

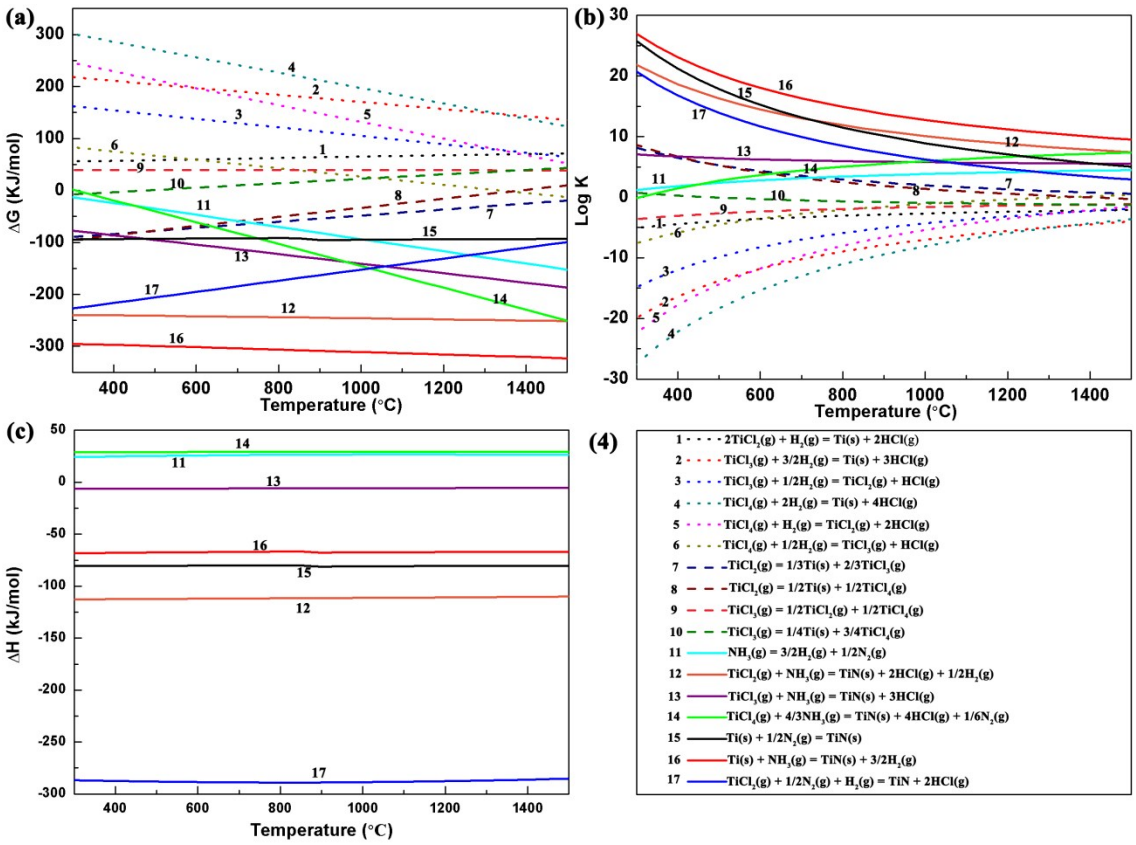

Fig. S6. Gibbs free energy variations (a) and the equilibrium constant variations (b) of the $TiCl_2$-NH_3 system at different temperatures. (c) The 17 possible reactions in the $TiCl_2$-NH_3 system.

VI. The crystal structure and surface energy of TiN

TiN is FCC interstitial compound with NaCl structure (Fig.S7). For FCC structured metals, such as Ag, Au, the surface energies (γ) can be roughly expressed by the following Eq.:[2]

$$\gamma = \frac{1}{2} N_b \varepsilon \rho_a \qquad (2)$$

where the N_b is the number of the broking bonds, ε is the bond energy, a is the cell parameters, and ρ_a is the atomic planar density. The faces with the lowest surface energy are the {111} facets, $\gamma\{111\} = 3.36(\varepsilon/a^2) < \gamma\{100\} = 4(\varepsilon/a^2) < \gamma\{110\} = 4.24(\varepsilon/a^2)$.[3] For FCC NaCl, the faces with the lowest surface energy are the {100} facets because of its ionic bond.[3] However, the bond structures of TiN are more

complicated than that of NaCl and Ag as the bonds are combination of ionic, covalent, and metallic contribution.[4] At present, the faces with the lowest surface energy in TiN are not well known.[3,5,6] The {111} planes of TiN are the exchange layers of pure Ti and pure N, which possess 2 Ti or N atoms (Fig. S7.a and c). The {100} planes of TiN possess 2 Ti atoms and 1 N atoms (Fig. S7.d and e). It has been reported that the growth rate of {111} planes is lower than that of {100} planes in the $TiCl_4$-NH_3 system.[3] Based on the Wulff's rule, crystal faces with high surface energies exhibit the fastest growth rates.[7,8] Hence, it is reasonable to predict that the faces with the lowest surface energy in TiN are the {111} facets.

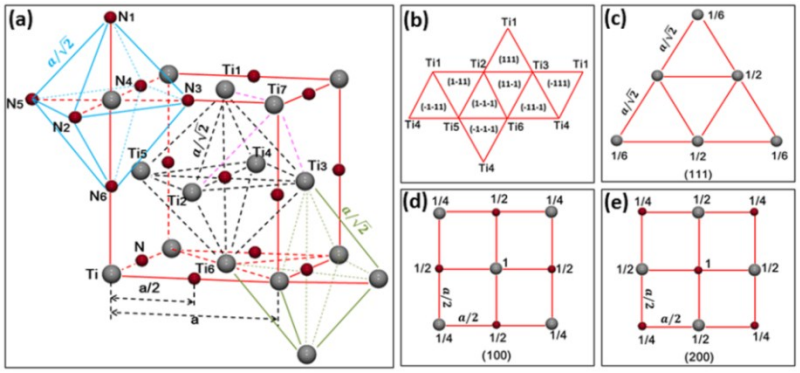

Fig.S7. (a) Schematic diagram of FCC structured TiN (grey balls represent Ti atoms, and deep red balls represent N atoms). (b) The expansion view of Ti1~ Ti6 octahedron with 8 {111} facets. (c) Schematic diagram of (111) plane. (d) and (e) Schematic diagrams of (100) plane and (200) plane, respectively.

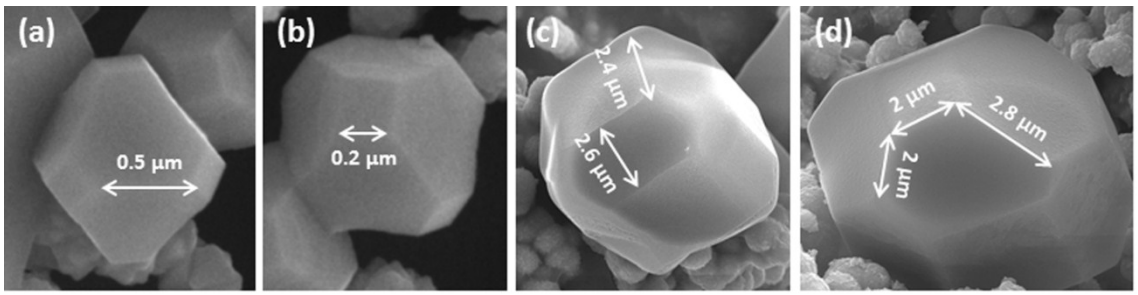

Fig.S8. The SEM images of truncated octahedra obtained from $TiCl_{2(g)}$-NH_3-Ar system at 850 °C (a and b) and 900 °C (c and d).

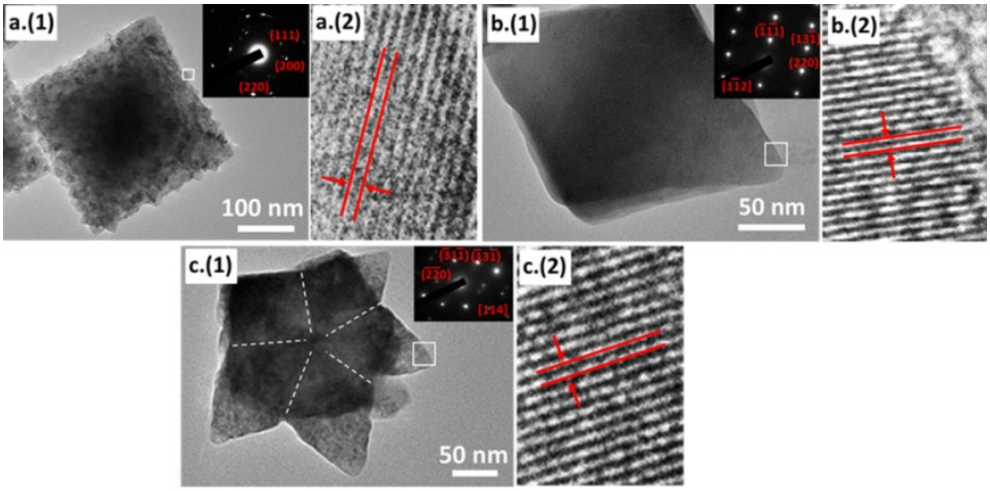

Fig.S9. TEM images (1), SAED patterns (insets), and HRTEM images (2) of the powders with octahedron shape. (a) The rough octahedron powder synthesized at 850 ^{o}C, (b) and (c) the smooth octahedron synthesized at 900 ^{o}C.

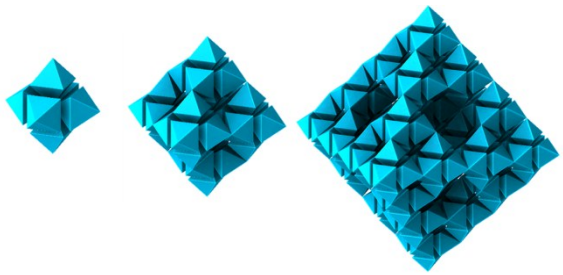

Fig.S10. Schematic diagram of the nanooctahedra oriented attachment by sharing the apex along [100] axes.

Fig.S11. Schematic diagram of 5 nanooctahedra oriented attachment by sharing the apex and {111}.

VII. References

1 J. S. Lee, J. M. Cha, H. Y. Yoon, J. K. Lee, Y. K. Kim, *Scientific Reports,* 2015, **5**, 12135.

2 Z. L. Wang, *J. Phys. Chem. B*, 2000, **104**, 1153–1175.

3 H. E. Cheng. M. H. Hon, *J. Appl. Phys.*, 1996, **79**, 8047–8053.

4 A. Neckel, The Physics and Chemistry of Carbides; Nitrides and Borides, edited by R. Freer (Kluwer Academic, Boston), 1990, 485–511.

5 J. Pelleg, L. Z. Zenvin, S. Lungo, *Thin Solid Films*, 1991, **197**,117–128.

6 C. Quaeyhaegens, G. Knuyt, J. D'Haen, L. M. Stals, *Thin Solid Films*, 1995, **258**, 170–173.

7 J. X. Fang, B. J. Ding, H. Gleiter, *Chem. Soc. Rev.*, 2011, **40**, 5347–5360.

8 M. Niederberger, H. Cölfen, *Phys. Chem. Chem. Phys.*, 2006, **8**, 3271–3287.